

Article

Effect of Titanium Based Alloys on Thermo-Mechanical Behavior in 3D Forging Simulation

Mohan Kumar Anand Raj ^{1,*}, Balaji Madheswaran ¹, Ali Jawad Alrubaie ², Hitesh Panchal ³, Suresh Muthusamy ⁴, Mustafa Musa Jaber ⁵, Chander Prakash ^{6,*}, Joao Paulo Davim ⁷, Kuldeep Kumar Saxena ⁸ and Dharam Buddhi ⁹

- ¹ Department of Mechanical Engineering, Kongu Engineering College (Autonomous), Perundurai 638060, India
² Department of Medical Instrumentation Techniques Engineering, Al-Mustaqbal University College, Hilla 51001, Iraq
³ Department of Mechanical Engineering, Government Engineering College, Patan 384265, India
⁴ Department of Electronics and Communication Engineering, Kongu Engineering College (Autonomous), Perundurai 638060, India
⁵ Department of Medical Instruments Engineering Techniques, Dijlah University College, Baghdad 10021, Iraq
⁶ School of Mechanical Engineering, Lovely Professional University, Phagwara 144001, India
⁷ Department of Mechanical Engineering, University of Aveiro, Campus Santiago, 3810-193 Aveiro, Portugal
⁸ Department of Mechanical Engineering, GLA University, Mathura 281406, India
⁹ Division of Research & Innovation, Uttaranchal University, Dehradun 248007, India
* Correspondence: mohankumar@kongu.ac.in (M.K.A.R.); chander.prakash@lpu.co.in (C.P.)

Abstract: Titanium has been one of the traditional metals used in the medical industry since 1940. This work modeled and simulated a hip-joint replacement implant using Creo 5.0 and DEFORM 3D (v11.0), respectively. Four titanium-based billets were modeled; out of four billets, three billets were coated with a specified thickness, and one was uncoated. Among the three coated billets, one billet was coated with a 500-micron and two billets coated with a 1000-micron thickness. At the end of the simulation, the coating materials formed patches on the surface of the forged parts. The coating material Ti-6Al-4V (high O₂) produced excellent mechanical properties in contrast to the CP-Ti material, which displayed low mechanical properties and did not match the core property. Hence, it was suggested to provide a bulk coating of Ti-6Al-4V (high O₂) on the billet to improve the physio-mechanical properties and biocompatibility. Four points were selected on the surface of the forged parts at different locations for identifying the property variations concerning forging time. Results found that coating thickness required more on the side surface of the billet material than on the upper and lower surfaces to enhance its properties.

Keywords: titanium alloy; Ti-6Al-4V ELI; Ti-6Al-4V (High O₂); CP-Ti; DEFORM 3D; partition billet



Citation: Raj, M.K.A.; Madheswaran, B.; Alrubaie, A.J.; Panchal, H.; Muthusamy, S.; Jaber, M.M.; Prakash, C.; Davim, J.P.; Saxena, K.K.; Buddhi, D. Effect of Titanium Based Alloys on Thermo-Mechanical Behavior in 3D Forging Simulation. *Metals* **2022**, *12*, 1611. <https://doi.org/10.3390/met12101611>

Academic Editor: Shoujin Sun

Received: 22 August 2022

Accepted: 20 September 2022

Published: 26 September 2022

Publisher's Note: MDPI stays neutral with regard to jurisdictional claims in published maps and institutional affiliations.



Copyright: © 2022 by the authors. Licensee MDPI, Basel, Switzerland. This article is an open access article distributed under the terms and conditions of the Creative Commons Attribution (CC BY) license (<https://creativecommons.org/licenses/by/4.0/>).

1. Introduction

The biomedical industry has been growing quickly for the last 33 years and has become essential to the medical industry [1]. Titanium-based material was introduced to the medical industry in the year 1940. Researchers implanted titanium, cobalt-chromium, and stainless-steel alloy in rat femurs and found no adverse effects. [2]. They continued research on titanium-based materials during the 1950s and ensured no adverse reactions [3,4]. Commercially pure titanium has been used successfully for bone plate and hip joint implants. Titanium alloy and Ti-6AL-4V were mainly used instead of different parts of knee and hip replacement joints. Specifically, this titanium-based material is used for structural load-carrying implants; it interacts with both bone and soft tissues. The tightness of the oxide layer formed next to the surface is measured by titanium-based metal biocompatibility. Well-defined bone has been displayed with resolution between 30 and 40 Å [3]. The conditions around the titanium-based metal implants were similar to ceramic implants. However, over a long period, metal becomes brittle and may lag off sufficient function [4].

The fibrous tissue layer forms between implants and surrounds; the thickness of the layer depends on the implant materials. In general, load-carrying implants are less biocompatible, but titanium and titanium-based alloys admit bio-compatibility due to their unique properties. Combining oxygen with a titanium alloy such as Ti-6Al-4V provides a very suitable material for medical applications; it is specified as extra low interstitial (ELI) [5]. Due to the manufacturing standards of medical implants, 0.13% of oxygen content is present in Titanium ELI material instead of the 0.2% standardized oxygen content [6].

The conventional method of manufacturing commercially pure titanium and titanium-based alloys is the forging process, which is the key manufacturing process for medical implants. According to the American Society of Testing and Materials (ASTM), standard implants are manufactured. The titanium-based materials are classified into five grades, the first four grades are pure titanium material, and the fifth grade is alloyed titanium. Among the five grades of titanium materials, Grade 2 and Grade 5 are applicable for medical fields; Grade 2 and 5 are applicable for dental and bone replacement implants, respectively. The Grade 5 material (Ti-6Al-4V) has higher tensile strength than other materials due to the presence of $\alpha + \beta$ alloy [7]. However, a few material drawbacks have also been reported, limited to medical applications. The commercially pure titanium and Ti-6Al-4V materials have lower wear-prevention properties and a higher Young's modulus than bone [8]. A few alloy materials, namely, niobium, tantalum, and zirconium are added to titanium to develop vanadium's cytotoxicity [9]. A low modulus of materials for implants is preferable because it prevents stress shielding [10]. Researchers reported that the heat treatment process obtained an enhanced hardness of β alloy materials [11]. The regulations for carrying out research work on forging titanium-based alloy materials reported in the literature [12] cite that the range of temperature to be maintained during the process is 900 to 1000 °C. The multibody forging process was investigated recently by investigators [13]; it consists of a stainless steel and aluminum alloy. The finite element method is used to analyze multibody components. Two different materials are combined and forged to a 6 mm distance to obtain enhanced bonding between materials. In this method, contact between the two materials is maintained by the penalty method [14].

Two or more materials are bonded together to form a single partitioned billet for the forging process. It provides the following advantages (1) enhancement of mechanical strength, (2) biocompatibility, and (3) microstructural properties. It is necessary to know about the manufacturing of such multi-partition billet material, with consideration of the requirements such as mechanical strength, biocompatibility, and microstructural properties. The different properties of the billet can also be attained through coatings and a suitable heat treatment process. The multi-partitioned billet can also be manufactured using rapid prototyping methods: direct layer deposition [15,16] and selective laser melting [17–19]. It can also be achieved by powder technology; a few drawbacks of powder technology are defects such as unprocessed powder presence during manufacturing causing a series of health problems.

This work focuses on the simulation of the physio-thermal analysis of hip replacement joints during the forging process. Furthermore, it compares single billets with multi-partition billets in terms of temperature distribution, stress, strain, deformation, and damage. The investigation was carried out through the finite element analysis method, The billet materials consist of four types, namely, Ti-6Al-4V ELI (Core), Ti-6Al-4V (high O₂), Ti-13V-11Cr-3Al and CP-Ti. Three software programs were used for the forging analysis, namely, Creo 5.0, DEFORM 3D (v11.0), and JMatPro. Future manufacturing will benefit from billet materials that meet the biocompatibility, mechanical strength, and microstructural criteria.

2. Materials and Methods

Three-dimensional modeling was created using modeling software Creo (5.0.0.0, Boston, MA, USA) [20], and physio-thermal analysis of the forging process was carried out using commercial finite element analysis software Deform (v11.0, Columbus, OH, USA). Billet dimensions were 220 × 55 × 23 mm³, a boxlike structure and used commercial upper

and lower dies for the forging operation of a hip joint replacement implant [20]. The coordinate system considered during the forging process was the x , y , and z axis, in which upper and lower dies were moved along the Z direction with a velocity of 2 mm/s. The upper and lower die were moved towards the negative and positive Z axes during the forging process. The total distance moved by the two dies was 23 mm. The finished hip joint replacement implant is shown in Figure 1a, obtained from the box-like billet. The initial billet, upper and lower dies are shown in Figure 1b. Emissivity and convective heat transfer between the surrounding air and billet material were 0.6 and $20 \text{ W m}^{-2} \text{ K}^{-1}$, respectively [5]. Coefficient heat transfer and friction coefficient between billet and die materials were $5000 \text{ W m}^{-2} \text{ K}^{-1}$ and 0.25, respectively [5]. The atmospheric and initial temperature of billet materials (Part 1, Part 2, and Part 3) were 20 and $970 \text{ }^\circ\text{C}$, respectively [12]. The initial temperature of the Part 4 material is set as $150 \text{ }^\circ\text{C}$. The upper and lower die material was a polycrystalline diamond with an atmospheric temperature of $20 \text{ }^\circ\text{C}$. The upper and lower dies moved simultaneously towards each other at the speed of 2 mm s^{-1} .

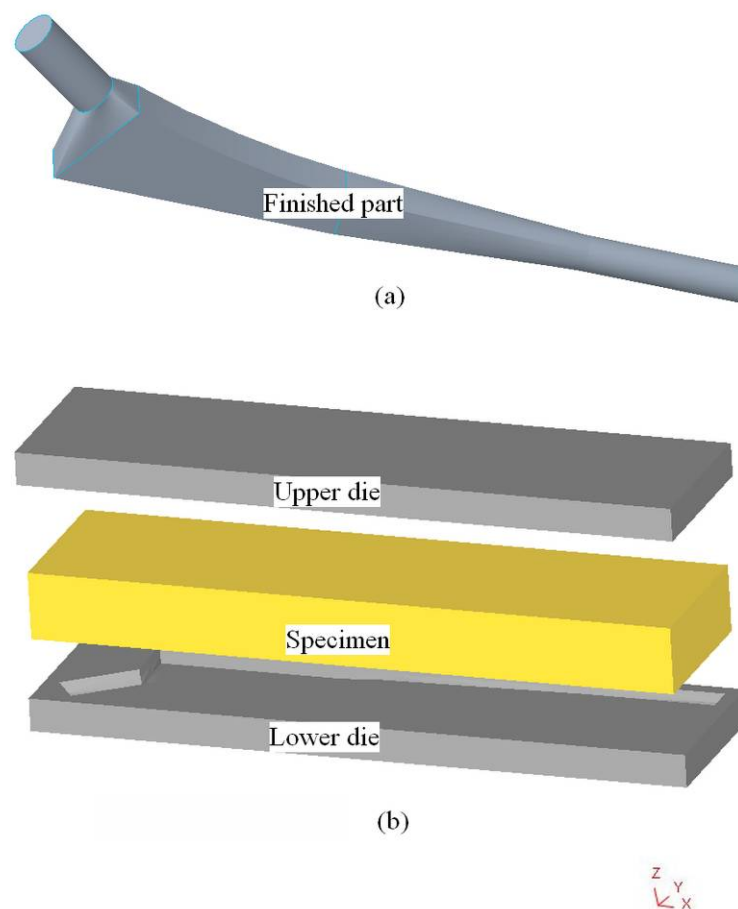
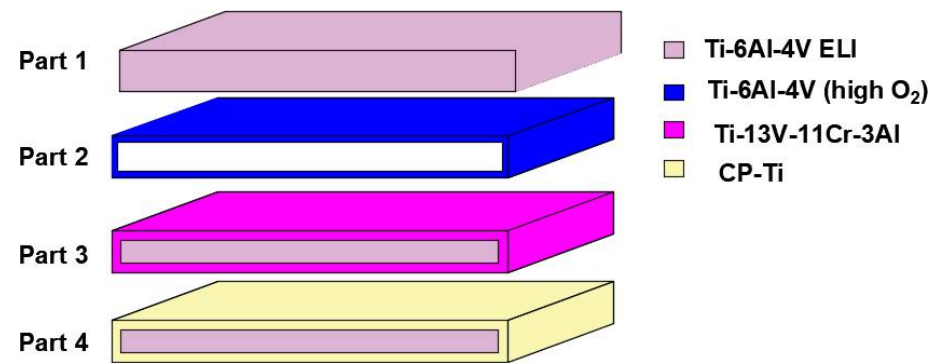


Figure 1. (a) Finished hip joint replacement implant for medical application, (b) initial billet and upper and lower dies for medical applications.

Different billet materials have been prepared and simulated. Three billets have shell material, and one billet is uncoated, as shown in Table 1. Partitioned billet materials are shown in Figure 2. Part 1 has assigned single material Ti-6Al-4V ELI throughout, which has maximum O_2 content of 0.13 weight%. The JMatPro materials modeling software was used for predicting flow stress, Poisson's ratio, specific heat, thermal conductivity, and Young's modulus, varying with temperature. The input and output parameters of the forging in DEFORM 3D software are shown in Table 2.

Table 1. Initial billet material condition.

Part	Description	Core	Shell
1	Single material	Ti-6Al-4V ELI	-
2	Core and Shell 1	Ti-6Al-4V ELI	Ti-6Al-4V (high O ₂)
3	Core and Shell 2	Ti-6Al-4V ELI	Ti-13V-11Cr-3Al
4	Core and Shell 3	Ti-6Al-4V ELI	CP-Ti (commercially pure titanium)

**Figure 2.** Billet is coated with different materials.**Table 2.** Input and output parameters of the forging in DEFORM 3D.

S. No	Input Parameter	Output Parameter (at Four Points)
1	Billet dimensions	Temperature distribution
2	Four points were chosen on the surface of billet	Effective stress
3	Velocity of billet	Induced damage
4	Total distance moved by the two dies	Strain and velocity
5	Emissivity and convective heat transfer	-
6	Coefficient of heat transfer and friction coefficient between billet and die materials	-
7	The atmospheric temperature and initial temperature of billet materials	-
8	Flow stress, Poisson's ratio, specific heat, thermal conductivity, and Young's modulus (Obtained from JMatPro software)	-

Part 2 consisted of two materials on the core and shell. The shell material Ti-6Al-4V (high O₂) was coated on the outer surface up to 0.5 mm, which had a higher oxygen pickup (0.5 weight%). The core part was material Ti-6Al-4V ELI. Part 3 had the same core material as model 2, but the shell material was replaced as Ti-13V-11Cr-3Al with a thickness of 1 mm. For Part 4, the material's outer shell was replaced with CP-Ti with a thickness of 1 mm. The internal core material was the same as other billet materials. The stress–strain relationship and physio-thermal properties of the titanium alloys are shown in Figures 3 and 4, respectively.

Sliding friction between dies and billet material was permitted with the 0.25 coefficient of friction; sliding between partition materials in the billet was not permitted. Titanium with higher oxygen pick-up material is very suitable for medical applications. In the bulk partition core and shell, materials were used in which the shell material had a higher oxygen pick-up property. The interface between the materials was introduced for the materials by either the Lagrange multiplier or penalty method [13,14]. Discretization of geometry and time steps allowed the physio-mechanical analysis of software to be computed accurately. For this work, minimum time steps were assumed as 0.05 s, and the number of elements varied from 1,50,000 to 2,40,000 due to the partition of materials.

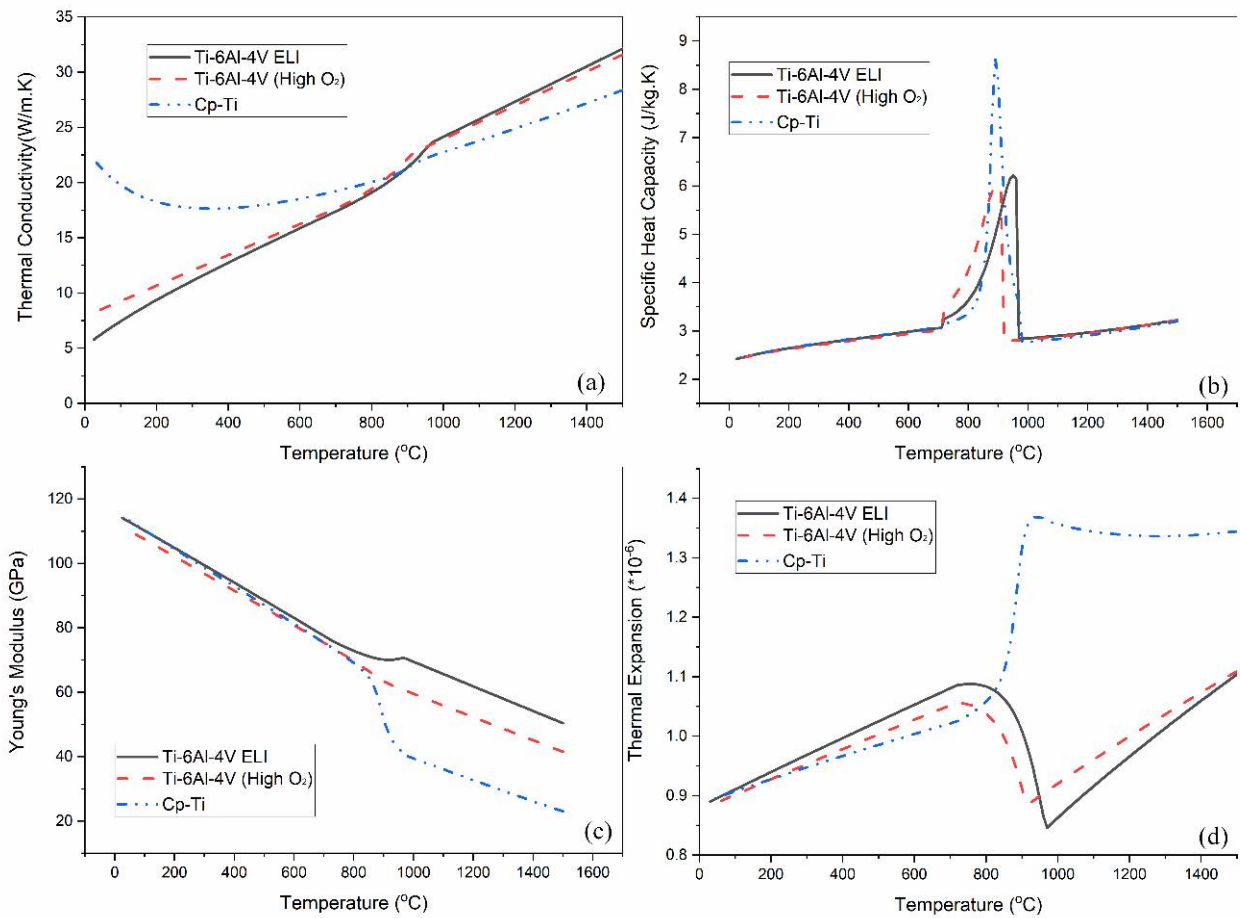


Figure 3. Physio-thermal properties vary with the temperature of Ti–6Al–4V ELI, Ti–6Al–4V (high O₂), and commercially pure titanium (Cp–Ti). (a) Thermal conductivity, (b) specific heat capacity, (c) Young’s modulus and (d) thermal expansion.

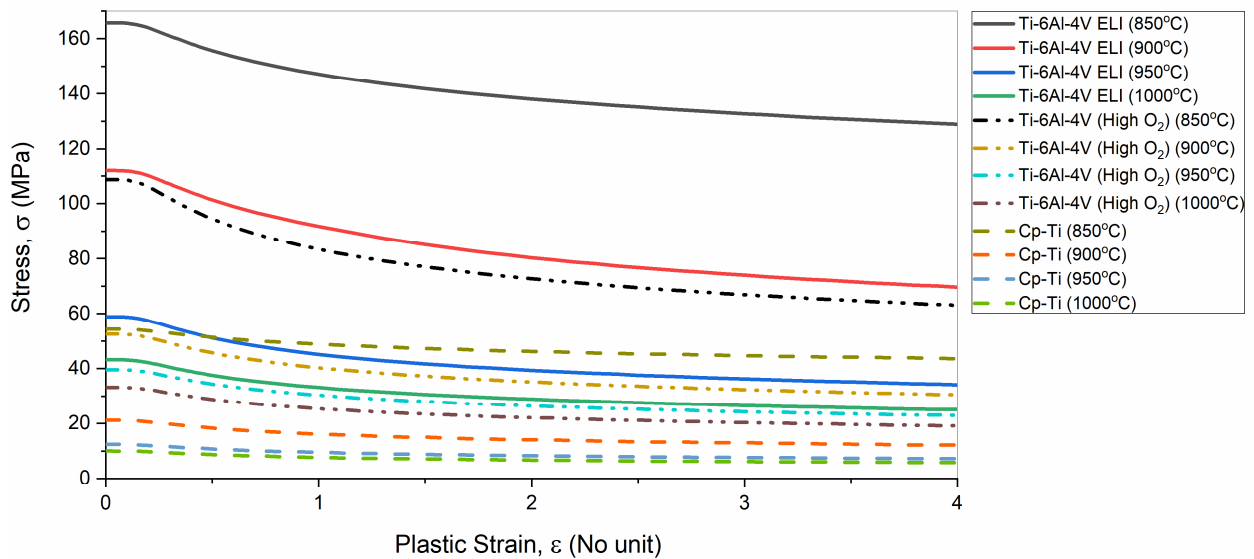


Figure 4. Stress–strain relationship of Ti-6Al-4V ELI, Ti-6Al-4V (high O₂), and commercially pure titanium (Cp-Ti) varies with temperature from 850 to 1000 °C.

3. Results

3.1. Mechanical Partition

The material partition at the end of the forging process of the hip joint implant is shown in Figure 5. It shows the surface texture of the billet material, blue and red indicate core and shell materials, respectively. Part 1 simulated up to 120-time steps with the material Ti-6AL-4V ELI as a single part. In Part 2, Ti-6Al-4V (High O₂) material added a coating thickness up to 500 microns to the initial billet; at the end of the forging process, the core material is exposed outside and forms a new surface. However, it is not exposed shell material on the outer surface. If it is needed for biocompatibility reasons, and the 500 microns have not produced a satisfactory result, this suggests a higher thickness of shell material.

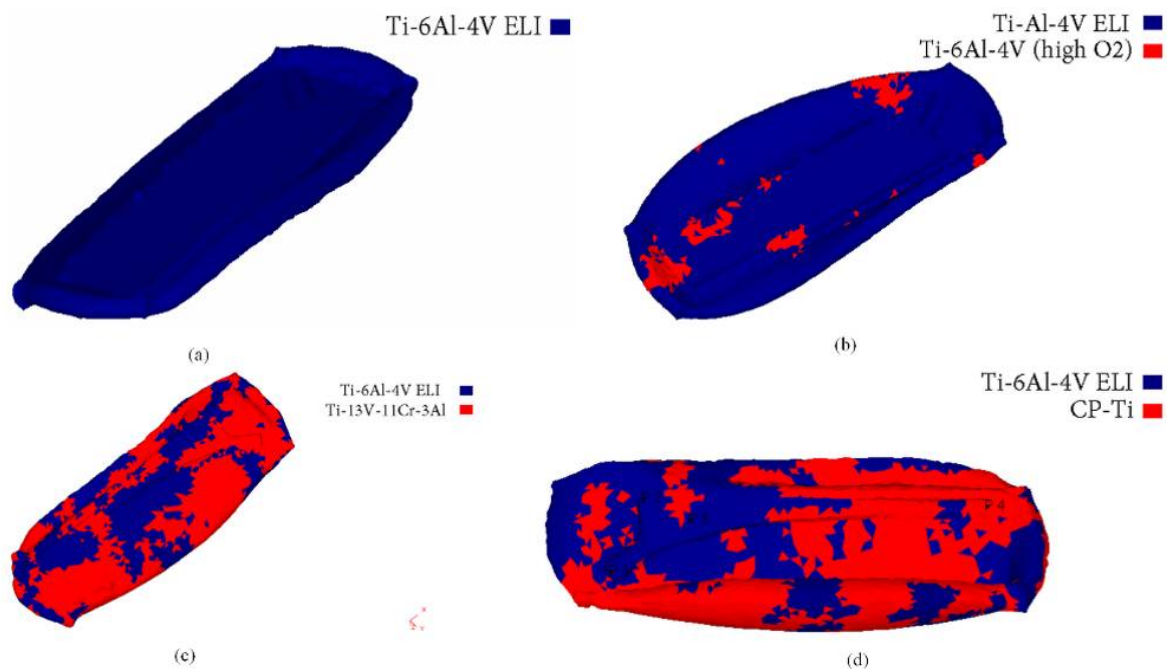


Figure 5. Three-dimensional view of partitioned forging of (a) Part 1, (b) Part 2, (c) Part 3 and (d) Part 4.

In Part 3, the core material used was the same. The shell material was replaced as Ti-13V-11Cr-3Al for the initial billet up to 1000 microns thick. The shell material was distributed on the outer surface as patches. CP-Ti material was used as shell material in Part 4, it is a softer material, and the flow stress behavior of this material differs from the core material (10 to 35% lower) [5,21–23]. The temperature range and strain rate of CP-Ti material were similar to the core material. At the higher temperature, it was easily separated from the core part with an even smaller applied load. At 850 °C, the CP-Ti material could withstand effective stress up to 54 MPa, as shown in Figure 4, which was 67% less than material Ti-6AL-4V ELI at the same temperature. The effective stress value gradually decreased when the temperature increased, as shown in Figure 4.

3.2. Properties Analysis of Finished Part at Different Points

Four points (P1, P2, P3, and P4) were selected for analysis on the forged hip joint, as shown in Figure 6. It is essential that remaining unwanted scrap material is removed from the forged parts to obtain the final finished product. A three-dimensional forging process was numerically computed in a physio-thermal environment. All physio-thermal properties have been computed using the software at each element and time step [24–29]. The final component was only the forging component that matched the finished part shown in Figure 1a; the remaining materials needed to be removed after the forging process as scrap.

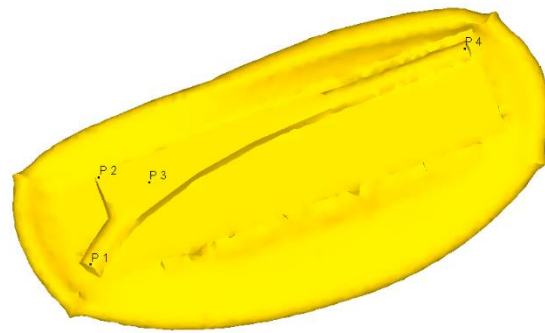


Figure 6. Four points (P1, P2, P3, and P4) are considered at different locations of the finished part of the hip joint for thermo-mechanical analysis.

The prediction of temperature distribution using the software after fixing the number of time steps and elements at different locations of the finished forging part is as shown in Figure 7. The total 120 time steps taken to complete the forging process, in which temperature losses from the initial temperature (970 °C) for Part 1, Part 2, and Part 3 as shown in Figure 7. For Part 4, the initial billet temperature was set at 150 °C due to the property difference between the core and shell materials, as shown in Figure 4. The Young's modulus of CP-Ti suddenly reduced by up to 30.64% between the temperatures of 860 to 920 °C, but in contradiction, the Young's modulus of the Ti-6AL-4V ELI (core) material increased by up to 2.98%. Similarly, the thermal expansion of CP-Ti values increased suddenly by up to 22.96% between the temperatures of 830 to 920 °C simultaneously, and the thermal expansion for the material Ti-6AL-4V ELI (core) dropped.

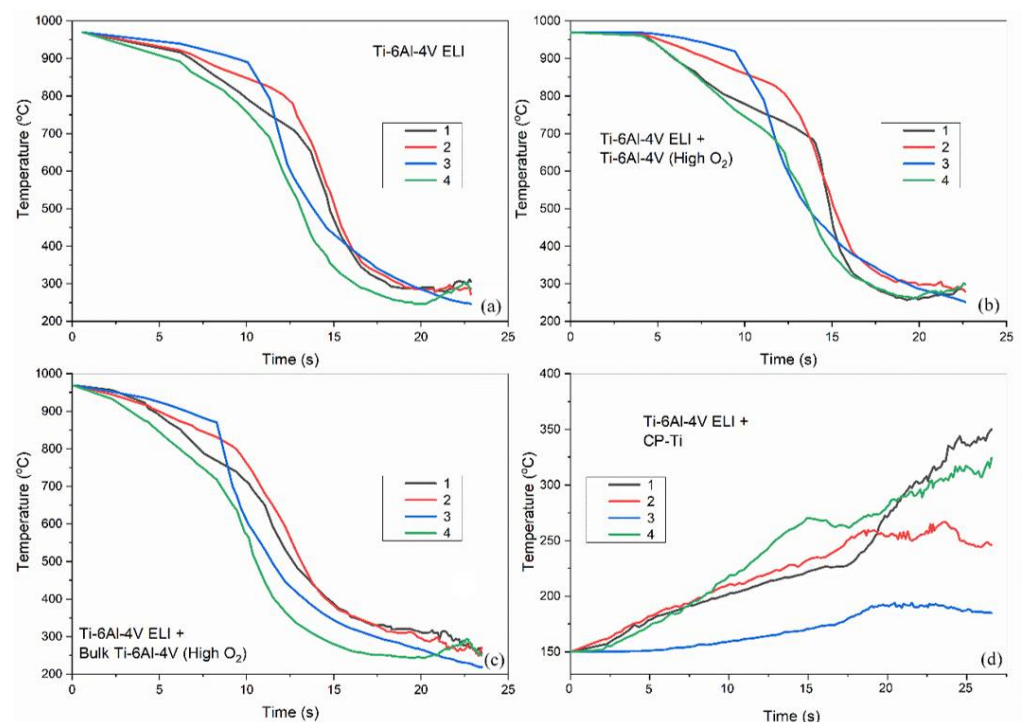


Figure 7. Temperature distribution at the four different points varies with time (a) Part 1, (b) Part 2, (c) Part 3, and (d) Part 4.

The temperature distribution of the forged parts is given in Figure 7. The temperature variations of four different points of the parts are shown in Figure 7a–d. Figure 7a displays the temperature variation of a single material (Ti-6AL-4V ELI) which varied temperatures with respect to time. Temperatures varied from 970 to 250 °C in the forging process's total duration (24 s). Figure 7b shows the initial temperature declined gradually up to

5s due to the presence of coating material (Ti-6AL-4V (high O₂)) up to 500 microns; after that, it reduced drastically from 800 to 350 °C during the forging process. It may be due to the higher thermal expansion and conductivity of Ti-6AL-4V ELI material. For all four points, P1, P2, P3, and P4, in Figure 7a,b, showed no significant differences in temperature distribution.

For Part 3, P3 is located in the middle of the forged part and had direct exposure to air rather than the upper die. Hence, the initial temperature was maintained for up to 15 s; after starting contact with the upper die material, the temperature reduced gradually due to direct heat transfer. P2 was close to the upper die. Direct heat transfer may be the reason for temperature variations, as shown in Figure 7c. In the case of Part 4, at the higher temperature, the shell materials had a very low thermal expansion and Young's modulus; the material deformed rapidly and pushed out all materials during the forging process. It may be the reason that the process was not able to perform at higher temperatures. Hence, the forging process should start at 150 °C. P3 maintained the same temperature up to 15 s, shown in Figure 7c; after that, the temperature reduced gradually, and the upper die and P3 did not have contact directly, which may be the reason for the steady-state temperature.

3.3. Effective Stress

Figure 8a,b displays a similar variation of effective stress to time. P3 was located in the middle of the forging part, it deformed freely due to direct contact with the upper die. At the initial temperature (970 °C), all the parts' points (P1, P2, P3, and P4) deformed freely up to 6s. When the temperature was reduced, particle movement was restricted; hence, effective stress increased drastically from 150 to 750 °C within 5 s, and stress gradually increased due to direct contact with dies. Figure 8c,d shows that all four points were increased gradually for the first 3s due to the coating material. It offered a lower load withstanding capacity compared to the core material after that; P3 gradually increased compared to other points (P1, P2, and P4) due to direct contact with the upper die material.

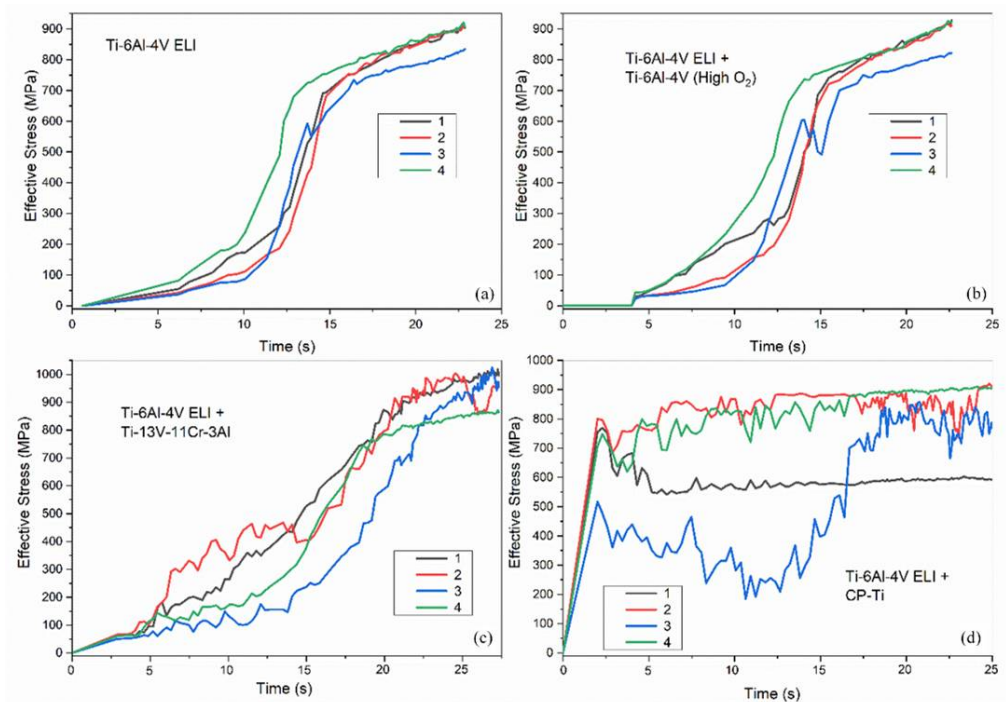


Figure 8. Effective stress at the four different points varies with time (a) Part 1, (b) Part 2, (c) Part 3, and (d) Part 4.

3.4. Damage, Velocity, and Strain

Figures 9–11 show the damage, velocity, and strain of the forged parts during the process, respectively. Damage induced during the forging process is shown in Figure 9a,d. A common observation shown in the graph was that P3 had a minimal chance of damage. Figure 9a,b shows that P2 had less chance of damage due to the higher mechanical strength of the materials. CP-Ti material had very low mechanical strength compared to the core material, hence a higher chance of damage occurrence for P2 than at other points.

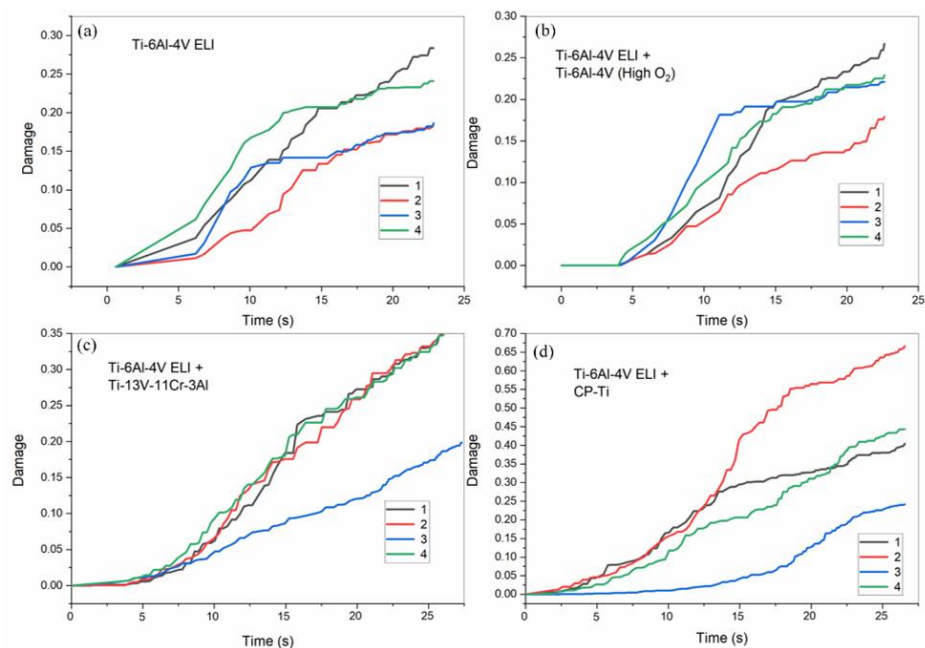


Figure 9. Damage induced during the forging process at the four different points (a) Part 1, (b) Part 2, (c) Part 3, and (d) Part 4.

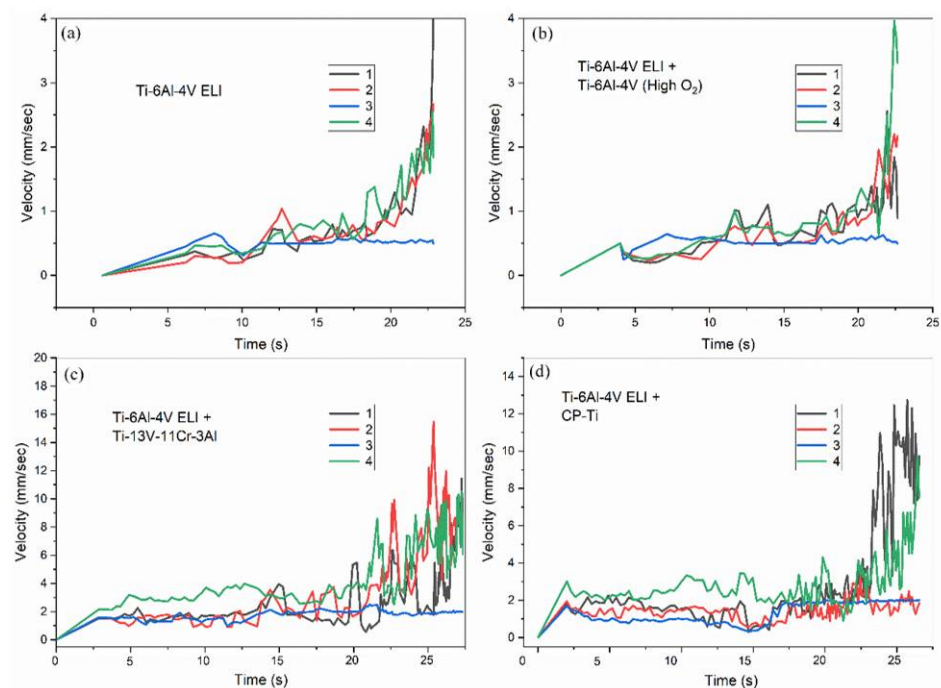


Figure 10. Velocity (rate of change of position of four points) at the four different points (a) Part 1, (b) Part 2, (c) Part 3, and (d) Part 4.

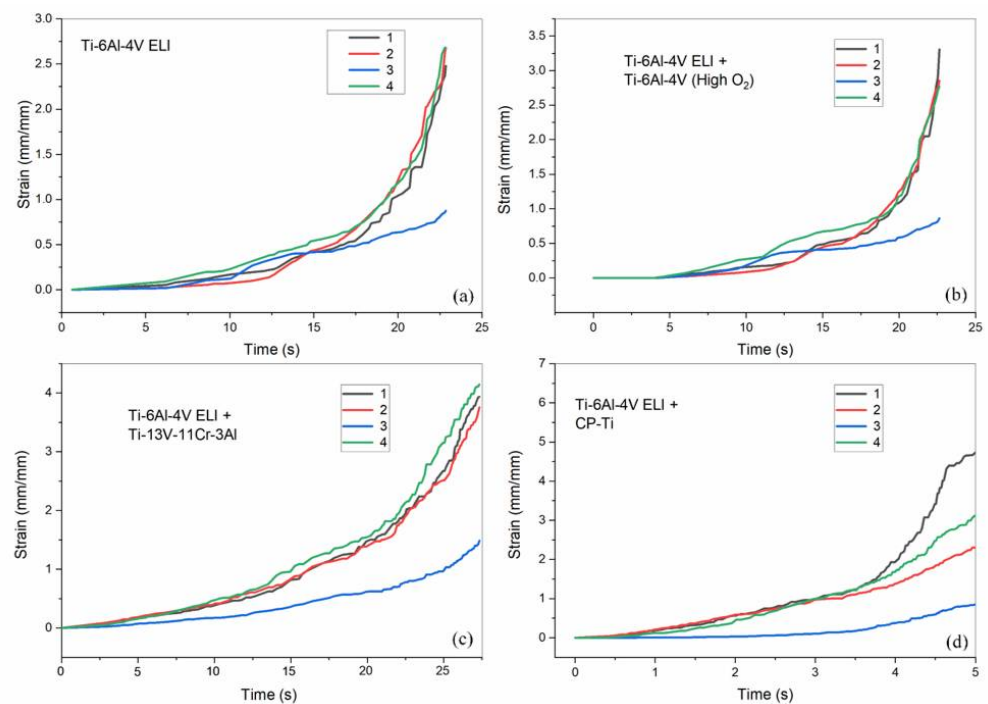


Figure 11. Strain at the four different points (a) Part 1, (b) Part 2, (c) Part 3, and (d) Part 4.

The velocity of P3 was almost maintained as constant in all cases shown in Figure 10a,d because P3 was not directly in contact with the upper die during the process. Due to the stability of the material at the higher temperature, the peak velocity reached 4 mm/s by point P4, as shown in Figure 10a,d. Due to the higher thermal expansion of the shell material, peak velocity reached 15 mm/s and 12 mm/s, as shown in Figure 11a,b, respectively. Strain produced in all cases is similarly shown in Figure 11a,d, due to free deformation P3 producing less strain compared to other points (P1, P2, and P4). The remaining points (P1, P2, and P4) produced similar strain values.

In this work, three software programs were used for the forging analysis, namely, Creo 5.0, DEFORM 3D (v11.0), and JMatPro. The initial billet and dies were modeled using Creo 5.0 and imported into DEFORM 3D software. The input parameters were used for the forging analysis: billet and die dimensions, moving velocity of dies and billet, Emissivity and convective heat transfer, coefficient of heat transfer, and friction coefficient between billet and die materials. The remaining specific properties of the materials, namely, flow stress, Poisson's ratio, specific heat, thermal conductivity, and Young's modulus, were obtained from JMatPro software. The output parameters were temperature distribution, effective stress, velocity, and strain. The four points (P1, P2, P3, and P4) were chosen for the study. These four points were chosen based on the high geometric concentration of the materials. The results showed that P3 in Part 2 produced good results compared to other materials. Due to the high thermal expansion and lower Young's modulus, Part 4 produced lower thermo-mechanical properties.

4. Conclusions

A hip joint replacement implant was modeled using Creo 5.0, and the forging process was simulated using DEFORM 3D (v11.0) software. Four different billet materials were used for the forging process; among the four billet materials, three materials were coated, and one was uncoated. In all the billet materials, the core part was the same (Ti-6Al-4V ELI), and the shell parts were different. The forging simulation was carried out using DEFORM 3D (v11.0) Software, the following results were obtained at the end of the analysis. Part 2 (Ti-6Al-4V (high O₂) as shell material) provided good results when the bulk shell thickness was used for the forging process. Four different points were considered at the

forged part's locations. Temperature distribution, effective stress, damage, velocity, and strain were predicted at the points. The results showed that P3 (located midpoint of the forged part) produced better results because the region was not directly in contact with the upper die up to 15s. P2 of Part 4 had a higher chance of damage occurring because the coating material (CP-Ti) had less mechanical strength than the other materials. The Cp-Ti material is not being suggested for the manufacturing of medical implants. The corners of the forged part required bulk coating rather than the middle region for improving physio-mechanical properties.

Author Contributions: Conceptualization, M.K.A.R.; methodology, B.M.; software, A.J.A.; validation, H.P.; formal analysis, S.M.; investigation, M.M.J.; resources, C.P.; data curation, J.P.D.; writing—original draft preparation, K.K.S.; writing—review and editing, K.K.S.; visualization, D.B.; supervision, M.K.A.R.; project administration, B.M.; funding acquisition, C.P., J.P.D., D.B. All authors have read and agreed to the published version of the manuscript.

Funding: This research received no external funding.

Institutional Review Board Statement: Not applicable.

Informed Consent Statement: Not applicable.

Data Availability Statement: Not applicable.

Conflicts of Interest: The authors declare no conflict of interest.

References

- Krishnan, R.; Pandiaraj, S.; Muthusamy, S.; Panchal, H.; Alsoufi, M.S.; Ibrahim, A.M.M.; Elsheikh, A. Biodegradable magnesium metal matrix composites for biomedical implants: Synthesis, mechanical performance, and corrosion behavior—A review. *J. Mater. Res. Technol.* **2022**, *20*, 650–670. [[CrossRef](#)]
- Singh, H.; Prakash, C.; Singh, S. Plasma spray deposition of HA-TiO₂ on β -phase Ti-35Nb-7Ta-5Zr alloy for hip stem: Characterization of bio-mechanical properties, wettability, and wear resistance. *J. Bionic Eng.* **2020**, *17*, 1029–1044. [[CrossRef](#)]
- Leventhal, G.S. Titanium, a metal for surgery. *JBJS* **1951**, *33*, 473–474. [[CrossRef](#)]
- Pramanik, A.; Basak, A.K.; Prakash, C. Understanding the wire electrical discharge machining of Ti6Al4V alloy. *Heliyon* **2019**, *5*, e01473. [[CrossRef](#)]
- Turner, R.; Antonic, J.; Warnken, N. 3D Forging simulation of a multi-partitioned titanium alloy billet for a medical implant. *J. Manuf. Mater. Process.* **2019**, *3*, 69. [[CrossRef](#)]
- Wienroth, M.; McCormack, P.; Joyce, T.J. Precaution, governance and the failure of medical implants: The ASR (TM) hip in the UK. *Life Sci. Soc. Policy* **2014**, *10*, 1–16. [[CrossRef](#)]
- Sidambe, A.; Choong, W.; Hamilton, H.; Todd, I. Correlation of metal injection moulded Ti6Al4V yield strength with resonance frequency (PCRT) measurements. *Mater. Sci. Eng. A* **2013**, *568*, 220–227. [[CrossRef](#)]
- Zhao, X.; Chen, J.; Lin, X.; Huang, W. Study on microstructure and mechanical properties of laser rapid forming Inconel 718. *Mater. Sci. Eng. A* **2008**, *478*, 119–124. [[CrossRef](#)]
- Bombač, D.; Brojan, M.; Fajfar, P.; Kosel, F.; Turk, R. Review of materials in medical applications Pregled materialov v medicinskih aplikacijah. *RMZ-Mater. Geoenviron.* **2007**, *54*, 471–499.
- Singh, S.; Prakash, C.; Singh, H. Deposition of HA-TiO₂ by plasma spray on β -phase Ti-35Nb-7Ta-5Zr alloy for hip stem: Characterization, mechanical properties, corrosion, and in-vitro bioactivity. *Surf. Coat. Technol.* **2020**, *398*, 126072. [[CrossRef](#)]
- Singh, S.; Prakash, C. Effect of cryogenic treatment on the microstructure, mechanical properties and finishability of β -TNTZ alloy for orthopedic applications. *Mater. Lett.* **2020**, *278*, 128461. [[CrossRef](#)]
- Adamus, J. Forming of the titanium implants and medical tools by metal working. *Arch. Mater. Sci. Eng.* **2007**, *28*, 313–316.
- Nielsen, C.V.; Zhang, W.; Martins, P.; Bay, N. Manufacturing Involving Forging of Multiple Objects in Contact. In Proceedings of the 6th JSTP International Seminar on Precision Forging, Kyoto, Japan, 11–14 March 2013.
- Babuška, I. The finite element method with penalty. *Math. Comput.* **1973**, *27*, 221–228. [[CrossRef](#)]
- Clark, D.; Whittaker, M.T.; Bache, M.R. Microstructural characterization of a prototype titanium alloy structure processed via direct laser deposition (DLD). *Metall. Mater. Trans. B* **2012**, *43*, 388–396. [[CrossRef](#)]
- Syed, W.U.H.; Pinkerton, A.J.; Li, L. Simultaneous wire-and powder-feed direct metal deposition: An investigation of the process characteristics and comparison with single-feed methods. *J. Laser Appl.* **2006**, *18*, 65–72. [[CrossRef](#)]
- Elsayed, M.; Ghazy, M.; Youssef, Y.; Essa, K. Optimization of SLM process parameters for Ti6Al4V medical implants. *Rapid Prototyp. J.* **2018**, *25*, 433–447. [[CrossRef](#)]
- Mohammed, M.T. Mechanical properties of SLM-titanium materials for biomedical applications: A review. *Mater. Today Proc.* **2018**, *5*, 17906–17913. [[CrossRef](#)]

19. Hallmann, S.; Glockner, P.; Daniel, C.; Seyda, V.; Emmelmann, C. Manufacturing of medical implants by combination of selective laser melting and laser ablation. *Lasers Manuf. Mater. Process.* **2015**, *2*, 124–134. [[CrossRef](#)]
20. Nandi, S.; Siddique, Z.; Cengiz Altan, M. A Grammatical Approach for Customization of Laminated Composite Materials. *Concurr. Eng.* **2011**, *19*, 157–174. [[CrossRef](#)]
21. Magargee, J.; Morestin, F.; Cao, J. Characterization of flow stress for commercially pure titanium subjected to electrically assisted deformation. *J. Eng. Mater. Technol.* **2013**, *135*, 041003. [[CrossRef](#)]
22. Reddy, N.; Lee, Y.H.; Park, C.H.; Lee, C.S. Prediction of flow stress in Ti-6Al-4V alloy with an equiaxed $\alpha + \beta$ microstructure by artificial neural networks. *Mater. Sci. Eng. A* **2008**, *492*, 276–282. [[CrossRef](#)]
23. Liu, R.; Hui, S.-X.; Ye, W.-J.; Li, C.-L.; Fu, Y.-Y.; Yu, Y.; Song, X.Y. Dynamic stress-strain properties of Ti-Al-V titanium alloys with various element contents. *Rare Metals.* **2013**, *32*, 555–559. [[CrossRef](#)]
24. Kumar, A.M.; Rajasekar, R.; Parameshwaran, R. 2D FEM simulation and experimental verification of Al 7075-T6 during turning process 2D-FEM-Simulation und experimentelle überprüfung von Al 7075-T6 während des Drehprozesses. *Mater. Und Werkst.* **2022**, *53*, 781–789. [[CrossRef](#)]
25. Mohan Kumar, A.; Parameshwaran, R.; Rajasekar, R. Simulation of 1.2765 DIN steel billet and crack analysis during the forging process using DEFORM 3D software. *Mater. Und Werkst.* **2021**, *52*, 332–338. [[CrossRef](#)]
26. Zhang, T.; Wei, D.; Lu, E.; Wang, W.; Wang, K.; Li, X.; Zhang, L.C.; Kato, H.; Lu, W.; Wang, L. Microstructure evolution and deformation mechanism of $\alpha + \beta$ dual-phase Ti-xNb-yTa-2Zr alloys with high performance. *J. Mater. Sci. Technol.* **2022**, *131*, 68–81. [[CrossRef](#)]
27. Wei, D.; Gong, W.; Wang, L.; Tang, B.; Kawasaki, T.; Harjo, S.; Kato, H. Strengthening of high-entropy alloys via modulation of cryo-pre-straining-induced defects. *J. Mater. Sci. Technol.* **2022**, *129*, 251–260. [[CrossRef](#)]
28. Cui, Y.W.; Chen, L.Y.; Qin, P.; Li, R.; Zang, Q.; Peng, J.; Zhang, L.; Lu, S.; Wang, L.; Zhang, L.C. Metastable pitting corrosion behavior of laser powder bed fusion produced Ti-6Al-4V in Hank's solution. *Corros. Sci.* **2022**, *203*, 110333. [[CrossRef](#)]
29. Raj, M.K.; Muthusamy, S.; Panchal, H.; Ibrahim, A.M.; Alsoufi, M.S.; Elsheikh, A.H. Investigation of mechanical properties of dual-fiber reinforcement in polymer composite. *J. Mater. Res. Technol.* **2022**, *18*, 3908–3915.